Ceramics International **23** (1997) 215–221

PII: S0272-8842(96)00028-4
0272-8842/97 $17.00+.00

Plasticity of Nanocrystalline Zirconia Ceramics and Composites

A. J. A. Winnubst, M. M. R. Boutz, Y. J. He, A. J. Burggraaf & H. Verweij

University of Twente, Faculty of Chemical Technology, Laboratory for Inorganic Materials Science, P.O. Box 217, 7500 AE, Enschede, The Netherlands

(Received 25 August 1995; accepted 12 September 1995)

Abstract: The deformation strain rate of nanocrystalline Y–TZP shows an increase by a factor 4 if the grain size decreases from 200 to 100 nm. Real superplastic deformation (strain rate $>10^{-4}$ s^{-1}) is observed in these materials at relative low temperature (1100–1200°C). Grain-boundary analysis indicates (partial) removal of an ultra-thin (1 nm), yttrium-rich grain boundary layer after deformation.

Uniaxial pressure-assisted sintering techniques (=sinter-forging) provide the opportunity of large shear strains during densification. Sinter-forging experiments on zirconia-toughened alumina (15 wt% ZrO_2/85 wt% Al_2O_3) resulted in a dense composite within 15 min at 1400°C and 40 MPa, with effective shear strains up to 100%. Sinter-forging of Y–TZP and ZTA gives an increase in strength, reliability and fracture toughness. These improvements are caused by the large shear strains that result from the removal of processing flaws. Also, the number of microcraks at the grain boundaries and the interatomic spacing between the grains are reduced by the forging techniques, resulting in a strengthening of the grain boundaries if compared with pressureless sintering. K_{IC} values of 10 MPa$\sqrt{m}$ are obtained for Y–TZP, while no classical stress-induced phase transformation toughening is observed. Sinter-forged ZTA samples showed a better wear resistance than free sintered ones.

1 INTRODUCTION

Superplasticity is defined as the ability of a crystalline material to undergo large elongations during tensile deformation.[1] Small grain sizes (<1 μm) lead to superplasticity in structural ceramics similar to the flow behaviour of superplastic metal alloys with grain sizes <10 μm. The ability of submicron-grained ceramics like Y–TZP to exhibit tensile elongations above 100% has made it possible to use various superplastic forming techniques to fabricate complex shapes with good dimensional control. In this way post-forming machining costs can be reduced substantially. The deformation behaviour of superplastic materials during this so-called "hot-forging" can be described by the phenomenological law:[1]

$$\dot{\epsilon} = A\frac{\sigma^n}{d^p}\exp\left(-\frac{Q}{RT}\right) \quad (1)$$

where $\dot{\epsilon}$ is the strain rate, A a numerical constant, σ the flow stress, n the stress exponent, d the grain size, p the grain size exponent, Q the apparent activation energy and RT has its usual meaning. From this equation it is clear that superplastic deformation rates can be enhanced by reducing the grain size to the nanocrystalline range, which can lead to industrial forming operations. Another method, often used to enhance superplasticity in ceramics, is the introduction of a glassy grain boundary phase.[1–3] In this way, a reduction of the operating temperature is possible because of an enhanced matter transport by the glassy phase. This glassy phase, however, is not beneficial for the electrical and (high temperature) mechanical properties.

A densification method, closely related to this "hot-forging" technique, is "sinter-forging". During sinter-forging a uniaxial pressure is applied to the specimen, without lateral constraint. In this way large creep strains are possible, which promote

densification. Residual flaws can be eliminated, provided appropriate forging conditions have been chosen. So sinter-forging may result in an improvement of the mechanical properties.

In this paper, the superplasticity of nanocrystalline single-phase zirconia and zirconia–alumina composites is described, starting from sinter-reactive powders, prepared by precipitation techniques. The influence of an externally applied stress at high temperatures during sintering, or in the dense state, on grain boundary properties, pore morphology and electrical, mechanical and tribological properties will be discussed.

2 EXPERIMENTAL PROCEDURE

The materials investigated were tetragonal ZrO_2 stabilized by doping with 2.6 mol% Y_2O_3 (= 2.6Y–TZP) and an Al_2O_3 composite doped with 15 wt% ZrO_2 (zirconia toughened alumina = ZTA). For both systems the powders were prepared by a gel precipitation technique in which metal chloride precursor solutions are hydrolysed in ammonia. After hydrolysis the gels were thoroughly washed with water/ammonia and ethanol, and subsequently dried and calcined in air for 2 h at 500°C for Y–TZP (crystallite size 8 nm) and at 900 or 1100°C for ZTA. More experimental details for Y–TZP are given in Ref. 4 and for ZTA in Ref. 5. Recently we have also performed a hydrothermal crystallization procedure on an Y–TZP gel at 190–205°C during 90 min under a nitrogen pressure of 2 MPa. These hydrothermally crystallized powders gave a more reproducible and an even better sinter-reactive powder than the air-calcined Y–TZP powders.[6]

After isostatic compaction at 400 MPa the samples were pressureless sintered, hot-forged or sinter-forged. Creep and sinter-forging tests were performed in air in a uniaxial hot-press using cylindrical or rectangular samples. Creep experiments were performed at 1100–1300°C under constant load with initial stresses in the range 20–120 MPa.[7]

Sinter-forging of the 2.6Y–TZP samples, as discussed in this paper, was performed under constant load at 1100°C, with initial stresses in the range 20–100 MPa. During sinter-forging of ZTA, the samples were heated to 1450°C at 2.5°C/min, while the pressure was linearly increased to 40 MPa in the temperature range of 1150–1200°C. An estimate of the effective shear (creep) strain was determined on the basis of the dimensional and density changes during sinter- or hot-forging of the compacts using the approach proposed by Raj.[8]

Grain boundaries were studied by Impedance Spectroscopy, XPS, Scanning Auger and TEM. More details are given in Refs 9 and 10. The (open) pore size distribution was analysed from N_2 adsorption/desorption isotherms and calculated from the adsorption branch, assuming cylindrical pores. Hg penetration porosimetry was used for pore sizes larger than 15 nm. Strength and fracture toughness were measured by 4-point bending and single edge notched beam, respectively.[11]

3 HOT-FORGING OF NANOCRYSTALLINE Y–TZP

The results of compression tests on 2.6Y–TZP samples are described extensively in Ref. 7. Two samples, with grain sizes of 0.1 and 0.2 μm, will be discussed in this paper. The initial relative density of the 0.1 μm sample (starting from a hydrothermally crystallized gel) equals 93% after (pressureless) sintering at 1085°C for 8 h,[6] while the 0.2 μm sample had a density of 98% after sintering at 1150°C for 10 h.[12] In Fig. 1, the stress vs strain rate curves during compaction at 1200°C are given for various ceramics. The results of the Y–TZP ceramics prepared in our group are denoted with (c) and (d) (0.2 and 0.1 μm, respectively), and are compared with several literature results. The stress exponent n [see eqn (1)] in all cases has a value near 2. The initial strain rate increases by a factor of 4 if the grain size decreases from 200 to 100 nm [Fig. 1 (c) and (d)]. From these preliminary results a grain size exponent $p = 2$ is calculated for this fine-grained region.

Examination of the microstructure by SEM after deformation at true strains of 0.50 indicates that the grains retained their equiaxed shape, while no (dynamic) grain growth took place.[7] This result, in combination with the creep parameters determined ($n = 2$, $Q = 480$ kJ/mol for 0.1 μm, $Q = 590$ kJ/mol for 0.2 μm), indicates grain boundary sliding as the dominant flow mechanism.[7,13] When compared with literature values for coarser grained (> 0.2 μm) systems, the value of Q is lower for the 0.1 μm system (480 instead of 550–600 kJ/mol). The grain size exponent p is mostly equal to 1 under the experimental conditions used (1100–1400°C and 20–120 MPa)[7] instead of 2, as is observed in the grain size region discussed here (0.1–0.2 μm). This difference in Q and p values is an indication for other, more favourable creep phenomena in the nanocrystalline regime (crystallite size < 200 nm). However, more deformation experiments are necessary to examine this phenomenon in detail.

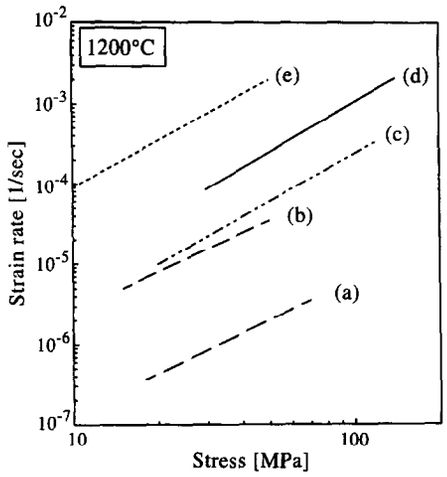

Fig. 1. Stress–strain rate of (a) 3Y–TZP, grain size $D = 0.4$ μm (Ref. 3), (b) 3Y–TZP + 1 wt% Ba-silicate, $D = 0.4$ μm (Ref. 3), (c) 2.6Y–TZP, $D = 0.2$ μm (this work), (d) 2.6Y–TZP, $D = 0.1$ μm (this work), and (e) 2Y–TZP + 0.3 mol% CuO, $D = 0.3$ μm (Ref. 2).

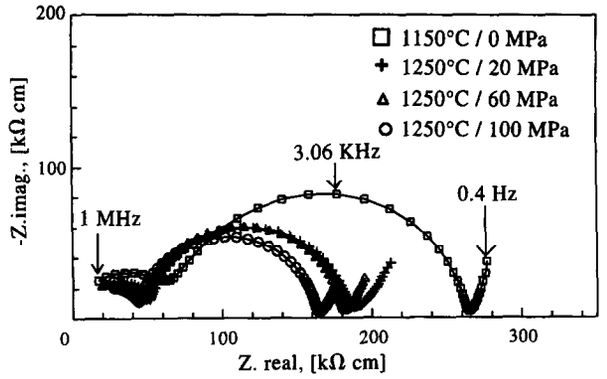

Fig. 2. Impedance spectra, measured at 340°C, of 2.6Y–TZP sintered at 1150°C or compressed at 1250°C.

From the results, it can be seen that real superplastic deformation (strain rate $> 10^{-4}$ s^{-1}) for ceramic materials at relatively low temperatures (1200°C) is possible for undoped Y–TZP at a stress of 50 MPa. By further reducing the grain size in the real nanocrystalline regime (< 100 nm), even higher strain rates are expected to be achieved.

In order to lower the temperature for superplastic deformation of coarser-grained systems (0.3–0.4 μm), amorphous or low melting-point grain boundary phases are often added to commercial Y–TZP materials.[2,3,14] In Fig. 1, strain rates are also given of commercial 3Y–TZP material (grain size 0.4 μm) with and without barium silicate glass addition,[3] and 2Y–TZP with 0.3 mol% CuO addition (grain size 0.3 μm).[2] The strain rate of the nanostructured material [(d) in Fig. 1] is one or two orders of magnitude higher than those of the other materials, except for the CuO-doped one, which shows the highest strain rate for Y–TZP as reported in literature. The CuO-containing grain boundary phase can, however, degrade the (high temperature) mechanical properties. The electrical (oxygen ionic) resistance also increases when impurities like CuO are added, as will be discussed in the next section.

3.1 Grain boundary characteristics

A complete analysis of the grain boundary characteristics is given in Refs 7, 9 and 10. After sintering at 1150°C, a thin (~1 nm thick) relatively "open" structure was observed by TEM, having an enrichment in Y and Si if compared with the grain bulk.[9] After deformation at 1250°C, the thickness of this grain boundary layer was reduced or almost disappeared. XPS analysis confirmed these results by a significant decrease in yttrium concentration at the grain boundaries after deformation at 1250°C.[9] So during hot-forging, a rearrangement of the atoms in the grain boundary occurs, resulting in a change in grain boundary morphology. This gives an improvement in grain boundary properties, such as strength of the grain boundaries and electrical (oxygen ion conducting) properties of the grain at boundaries. This last item will now be discussed.

In Fig. 2, complex impedance spectra (recorded at 340°C) are shown of 2.6Y–TZP after pressureless sintering at 1150°C (10 h) and after subsequent compression at 1250°C to 50% of the original length under initial stresses of 20, 60 and 100 MPa. The deformation time was, respectively, 120, 30 and 20 min. The average grain size was in the range of 0.21–0.24 μm.[9] So in this case, there was also no observable dynamic grain growth. The impedance spectra were analysed using the brick-layer model proposed by van Dijk and Burggraaf.[15] The semi-circles shown in Fig. 2 are ascribed to grain boundary dispersion. The (overall) grain boundary resistance corresponds to the distance between the intercepts of this grain boundary semi-circle on the Z-real axis. The high frequency intercept (at low Z-real) corresponds with the grain-bulk resistance. No change in grain-bulk resistance is observed after deformation, indicating that hot-forging does not influence the grain-bulk properties. However, the grain boundary resistance decreases by 50% after a subsequent deformation at 1250°C of a 1150°C sintered specimen. This decrease in grain boundary resistance can be caused in two ways. First the temperature treatment itself (without applying an external force) can result in a decrease in grain boundary resistance. Secondly, hot-forging in itself has a positive effect on grain boundary resistance, which can be seen from the lower grain boundary resistance at higher loads (100 MPa; see

Fig. 4). This difference can be explained in terms of reduction of the grain boundary thickness or partial removal of a continuous, poorly oxygen-ion conducting grain boundary layer.[9,16]

The addition of CuO to Y–TZP gives an increase in strain rate [Fig. 1(e)], but also gives a drastic increase (by a factor of 10–15) in grain boundary resistance, while the grain-bulk resistance remained unchanged if compared with pure Y–TZP.[17] This negative effect of impurities on grain boundary conductivity of yttria-doped zirconia systems has been observed for several dopants.[18] Deformation of the CuO-doped samples gives no improvement of the grain boundary resistance,[17] indicating that the grain boundaries remain covered by a CuO-rich layer after deformation. From these results it can be concluded that superplastically deformed CuO-doped Y–TZP [Fig. 1(e)], cannot be used in electronic devices like oxygen sensors and solid oxide fuel cells.

4 SINTER-FORGING OF Y–TZP AND ZTA

In Table 1, the sinter times necessary for obtaining a dense (92–94%) 2.6Y–TZP ceramic at 1100°C are given. From this table it is clear that this time decreases drastically when the initial load increases from 0 MPa (free sintering) to 84 MPa. Again, no dynamic grain growth is observed, even at an initial stress of 84 MPa. After reaching 93–94% relative density, creep occurs without further densification during sinter-forging at 1100°C.[19]

Figure 3 shows the stress dependence of the creep strain rate of Y–TZP with a grain size of 0.1 μm during sinter-forging (density 85–90%) or hot-forging (density 95%). The stress exponent of a sinter-forged sample is very close to the value of the hot-forged one ($n \sim 2$), indicating that the same mechanism (interface-reaction-controlled creep) is rate limiting during creep in both dense and porous materials.[7,19] The porous material still has a higher strain rate if strain rates of porous and dense Y–TZP are compared with identical grain sizes. The porosity, therefore, results in an extra creep strain rate. This influence of porosity on creep will be discussed in Section 4.1.

Table 1. Sinter time of Y–TZP at 1100°C as a function of applied load

Initial load (MPa)	Time (min)	Relative density (%)	Grain size (μm)
0	900	92	0.18
28	160	94	0.13
58	50	94	—
84	22	94	0.10

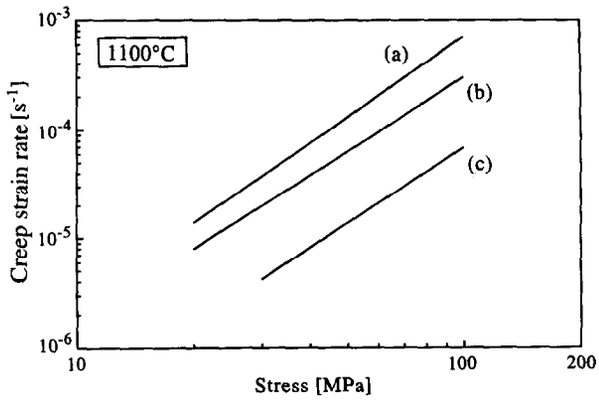

Fig. 3. Stress vs strain rate for 2.6Y–TZP at 1100°C with various densities (grain size 0.1 μm): (a) 85%, (b) 90%, (c) 95%.

Sinter-forging of ZTA powder compacts also has a strong beneficial effect on densification, while large creep strains are achieved. The results are summarized in Table 2. From this table it can be seen that sinter-forging at an initial stress of 40 MPa results in a dense (98+%) ZTA ceramic at a lower temperature (and within a shorter time) if compared with pressureless sintered samples (0 MPa). The alumina and zirconia grain sizes after sinter-forging at 1400°C (15 min) are 0.7 and 0.2 μm, respectively, while the smallest average grain sizes obtained after pressureless sintering are 0.8 and 0.3 μm, respectively. After sinter-forging, no textural development, such as preferential orientation during grain growth, is observed. The results in Table 2 show that during pressureless sintering (0 MPa) the densification behaviour is dependent on the powder calcination temperature, as is discussed by Den Exter *et al.*[5] This calcination temperature dependence is not observed during sinter-forging. This can be explained by the pore morphology development during sintering and will be discussed in the next section.

In Fig. 4, the volume strain (densification) and creep strain of the two types of ZTA compacts are given during heating at 2°C/min. Here it is also visible that the powder calcination temperature influences the free sintering behaviour, while this is not the case for sinter-forging. Another result which can be seen from this figure is that the dense material (no increase in volume strain) can

Table 2. Minimum sinter temperature/time schedule for dense (98%) ZTA as a function of load

T_{calc} powder (°C)	Load (MPa)	Sinter temp./time	Creep strain (ε_e)
900	0	1500°C/2 h	0
900	40	1400°C/15 min	0.79
1100	0	1450°C/2 h	0
1100	40	1400°C/15 min	0.80

undergo creep strains of more than 100% just by heating to 1450°C. So these ZTA materials show interesting superplastic-forming possibilities.

4.1 Pore morphology development during sinter-forging

In the previous paragraph it is discussed that sinter-forging strongly reduces temperature and time for obtaining a dense ceramic. This improvement compared with free sintering is not only due to the observed creep strain during sinter-forging in the final stage. In addition to this, the pore morphology development during the initial and/or intermediate sintering stage (with open porosity) is influenced by applying an external pressure.

The evolution of pore size distribution (= PSD) of several 2.6Y–TZP samples was investigated after free sintering and sinter-forging at 1100°C of 2.6Y–TZP. All samples had a relative density of approximately 80% and a crystallite size of about 40 nm. The density of 80% was achieved by varying the sintering time as a function of applied stress. N_2 physical adsorption indicated cylindrical pores. The pore size distribution could be determined more accurately by Hg porosimetry and is given in Fig. 5. From this figure it can be seen that a very broad PSD is observed in the free sintered material. After sinter-forging the volume of pores with radii 15–17 nm increases strongly, while small pores (radius < 10 nm) disappear progressively at increasing stress. This means that the pore size to grain size ratio is more uniform, resulting in a more homogeneous densification in the compact. In the free sintered compact, this ratio is strongly varying over the compact giving inhomogeneous densification and consequently local differential stresses inhibiting further densification.

A possible mechanism for the disappearance of the smaller pores during sinter-forging is coalescence to form larger pores. This reorganisation to a more homogeneous compact is likely to cause the extra creep strain rate for porous systems if compared with dense (hot-forged) Y–TZP, as indicated in Fig. 4.

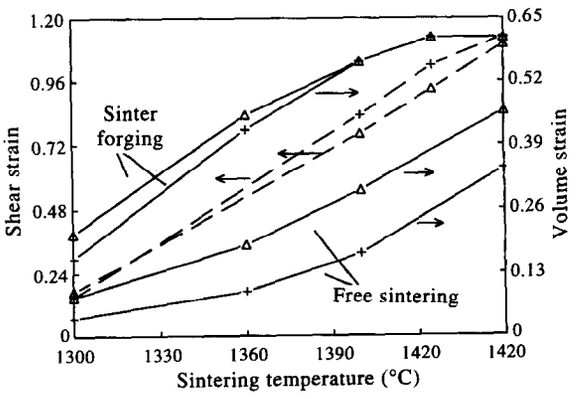

Fig. 4. Shear strain (dotted line) and volume strain (solid line) during sinter-forging of ZTA at 40 MPa. (Δ): calcined at 1100°C, (+): calcined at 900°C.

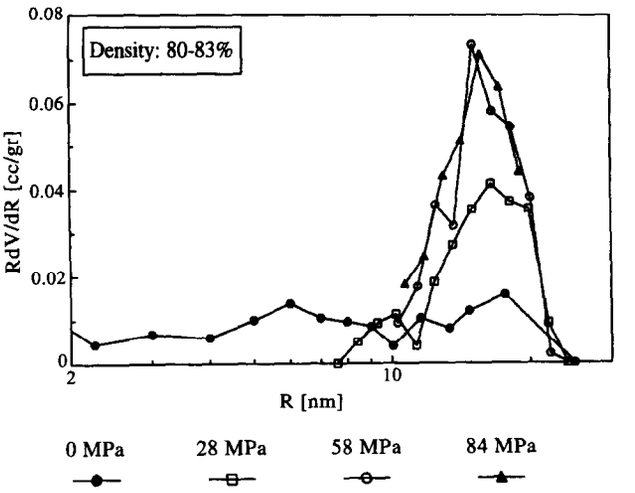

Fig. 5. Pore size distribution of Y–TZP with 80–83% relative density after sintering under several initial stresses as indicated.

The influence of applied stress on pore morphology development during the initial sintering stage in ZTA is illustrated in Fig. 6. During this sintering stage a slight densification occurs. The main phenomenon in this temperature region is the phase transformation from θ to α-Al_2O_3 at around 1250°C. During this phase transformation a rearrangement of the pore morphology occurs.[5] In Fig. 6 the pore size distribution just after the θ → α-Al_2O_3 transformation is given for a powder compact calcined at 900°C. There is a slight increase in pore size when the sample is sinter-forged, but the main difference between sinter-forging and free sintering is the presence of the broad tail of small pores

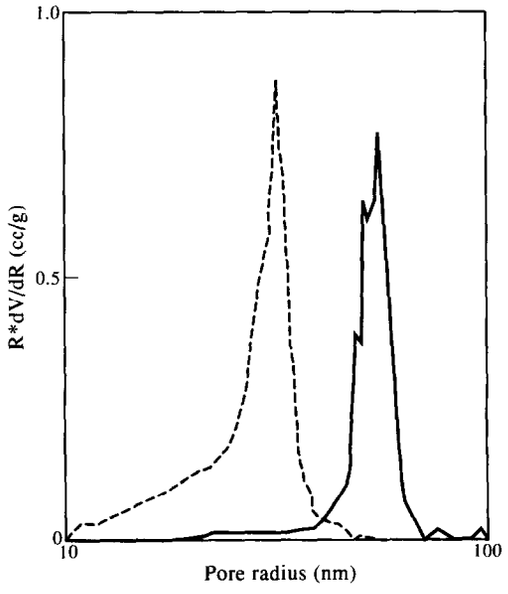

Fig. 6. Pore size distribution of a ZTA compact after phase transformation (T_{sinter} = 1250°C). Dotted line: free sintered, solid line: sinter-forged.

in the free sintered compact. These small pores are remainders of intra-aggregate pores of the porous θ-alumina aggregates.[5] After the phase transformation, the pressureless sintered 900°C calcined compact consists of irregularly shaped α-Al_2O_3 crystallites with irregularly shaped pores.[5] The external pressure during sinter-forging results in shear deformation and internal reorganisation during the θ → α-Al_2O_3 phase transformation. This provides the opportunity to eliminate the small intra-aggregate pores and transform them to larger inter-aggregate pores.[20] In this way a more homogeneous microstructure can be obtained after further densification.

From these results it is shown that not only do high creep strains during the final stage of sinter-forging result in an enhancement of densification compared with free sintering, a rearrangement to a more homogeneous microstructure in the state of open porosity is also important for a beneficial sintering behaviour.[20]

4.2 Mechanical and tribological properties of sinter-forged ceramics

The mechanical properties of both types of zirconia ceramics were strongly enhanced by sinter-forging. First the results of dense (98%) 2.6Y–TZP samples with a grain size of 0.2 μm will be discussed. This microstructure was obtained after free sintering for 10 h at 1150°C or after sinter-forging for 25 min at 1150°C at an initial stress of 80 MPa (total creep strain after sinter-forging: 0.3). The 4-point bending strength of free sintered and sinter-forged 2.6Y–TZP were found to be 454 ± 110 and 526 ± 21 MPa, respectively. These relatively low values are probably caused by cracks at the sharp edges of the samples which arose during machining and were not removed prior to mechanical testing. For sinter-forged samples a slight increase in strength and a better reproducibility were observed. The fact that sinter-forging has a beneficial effect on reliability is best demonstrated by the increase of the Weibull modulus (m) from 10 (free sintered) to 21 (sinter-forged) as calculated from 8 measurements. Since strength and reliability are sensitive to the presence of flaws, it is clear that in this Y–TZP system the flaw size and concentration are reduced by sinter-forging. A value of $m = 21$ indicates that these materials can be used as a reliable construction ceramic.

The fracture toughness of this 2.6Y–TZP sample increases after sinter-forging from 8 to 10 MPa$\sqrt{m}$. The crystal structure of the ceramic bulk, as well as the fractured surface of these TZPs, was found to be 100% tetragonal. The toughening mechanism which caused the high fracture toughness and strength values can therefore not be ascribed to an (irreversible) stress-induced phase transformation of tetragonal to monoclinic zirconia. Possible mechanisms for explaining the toughening in this very fine grained Y–TZP are reversible phase transformation, ferroelastic domain switching and crack deflection. It is interesting to study in more detail the toughening mechanism in this nanocrystalline, plastically deformable material and to investigate the mechanical properties of Y–TZP with grain sizes < 100 nm.

For ZTA samples the mechanical properties after free sintering (2 h) and sinter-forging (15 min, 40 MPa) at 1450°C will now be given. A more comprehensive description of the results is given by He *et al.*[21] All samples had a relative density of 98–99% and a zirconia and alumina grain size of 0.3 and 0.8 μm, respectively. After sinter-forging the total creep strain amounted to more than 100% (see also Fig. 4). The fracture toughness values of free sintered and sinter-forged ZTA were found to be 5.2 ± 0.1 and 7.4 ± 0.4 MPa$\sqrt{m}$, respectively, while the strength values were 380 ± 90 and 770 ± 90 MPa, respectively. Fracture toughness increases by 50% and strength increases by 100% if the ZTA samples are sinter-forged. The increase in strength indicates that flaws are effectively removed by the large creep strains.

XRD analysis showed that most of the zirconia particles in the bulk ZTA ceramic are in the tetragonal form, while after fracture 30 vol% of the zirconia at the fractured surface is transformed to monoclinic zirconia. The amount of transformed zirconia is not influenced by sinter-forging. So the contribution of stress-induced phase transformation as a toughening mechanism is the same for both systems. The difference in mechanical properties indicates that for the sinter-forged samples an extra toughening mechanism occurs. All samples fracture inter-granularly, so the difference in mechanical properties can be ascribed to a difference in grain boundary properties. Krell and Blank[22] introduce a microscopic grain boundary energy and a microscopic grain boundary toughness (K_{1C}^{gb}) concept in order to understand the improvement in toughness and strength by improving grain boundary structures. K_{1C}^{gb} increases with decreasing grain boundary porosity and decreasing amount of an amorphous grain boundary phase.[22] The large creep strain observed in our samples can result in partial de-wetting of the grain boundaries, as was observed by Boutz *et al.* after sinter-forging of Y–TZP, or in a reduction of interatomic distances in the grain boundary.[9] This improved grain boundary structure results in an increase in K_{1C}^{gb} [2,3] and, consequently, in an

increase in K_{IC}. Wear tests on a (SiC) ball on (ZTA) plate tribometer under a Hertzian contact pressure of 858 MPa showed a decrease in wear rate if the ZTA samples were sinter-forged.[23,24] Sinter-forged and free sintered samples have a wear rate of, respectively, 1.4×10^{-6} mm^3/Nm and 3.4×10^{-6} mm^3/Nm.[23,24] This reduction in wear loss can be explained by the strengthening of the grain boundaries and the reduction of (micro) defect size and concentration by means of sinter-forging.

5 CONCLUSIONS

The following conclusions can be drawn from the work described in this paper:

- Pressureless sintering (8 h at 1085°C) of a nanocrystalline Y–TZP powder compact results in a dense ceramic with a grain size of 100 nm.
- Real superplastic deformation (strain rate $> 10^{-4}s^{-1}$) of this ceramic is possible at relatively low temperatures (1200°C) and a stress of 50 MPa. No dynamic grain growth is observed.
- By applying an extra stress during sintering (= sinter-forging) even larger creep strains are observed in Y–TZP. During sinter-forging a more homogeneous pore structure is obtained in the intermediate sintering stage.
- Sinter-forging of ZTA powder compacts, starting from θ-Al_2O_3, shifts the densification to lower temperatures, compared with pressureless sintering. Creep strains of 100% are achieved after sinter-forging for 15 min at 1450°C
- The pore size distribution in the compact just after the $\theta \rightarrow \alpha$-$Al_2O_3$ phase transformation is more uniform after sinter-forging. This rearrangement in the porous compact is a better start for further densification.
- Strength, toughness and reliability (Weibull modulus) can be drastically increased by sinter-forging. For Y–TZP, K_{IC} values of 8–10 MPa$\sqrt{m}$ are measured, whereas no stress-induced (irreversible) phase transformation is observed. After sinter-forging Y–TZP the Weibull modulus had a value of 21. In ZTA, the strength increases by a factor of 2 to 770 MPa after sinter-forging. The (micro) defect size and concentration is decreased by sinter-forging.
- Pressure-assisted heat treatments (sinter- or hot-forging) result in better grain boundary morphologies. The grain boundary resistivity slightly decreases, while the (grain boundary) toughness increases in this way.
- Wear loss in ZTA decreases by more than a factor of 2 if the sample is sinter-forged.

REFERENCES

1. CHEN, I.-W. & XUE, L. A., *J. Am. Ceram. Soc.*, **73** (1990) 2585–2609.
2. HWANG, C. J. & CHEN, I.-W., *J. Am. Ceram. Soc.*, **73** (1990) 1626.
3. GUST, M., WOLFENSTINE, J. & MECARTNEY, M. L., *J. Am. Ceram. Soc.*, **76** (1993) 1681.
4. GROOT ZEVERT, W. F. M., WINNUBST, A. J. A., THEUNISSEN, G. S. A. M. & BURGGRAAF, A. J., *J. Mater. Sci.*, **25** (1990) 3449.
5. DEN EXTER, P., WINNUBST, A. J. A., LEUWERINK, T. H. P. & BURGGRAAF, A. J., *J. Am. Ceram. Soc.*, **77** (1994) 2376.
6. BOUTZ, M. M. R., OLDE SCHOLTENHUIS, R. J. M., WINNUBST, A. J. A. & BURGGRAAF, A. J., *Mater. Res. Bull.*, **29** (1994) 311.
7. BOUTZ, M. M. R., WINNUBST, A. J. A., BURGGRAAF, A. J., NAUER, M. & CARRY, C., *J. Eur. Ceram. Soc.*, **13** (1994) 103.
8. RAJ, R. J., *J. Am. Ceram. Soc.*, **65** (1982) C46.
9. BOUTZ, M. M. R., CHEN, C. S., WINNUBST, A. J. A. & BURGGRAAF, A. J., *J. Am. Ceram. Soc.*, **77** (1994) 2632.
10. CHEN, C. S., BOUTZ, M. M. R., BOUKAMP, B. A., WINNUBST, A. J. A., DE VRIES, K. J. & BURGRRAAF, A. J., *Mater. Sci. Eng.*, **A168** (1993) 231.
11. THEUNISSEN, G. S. A. M., BOUMA, J. S., WINNUBST, A. J. A. & BURGGRAAF, A. J., *J. Mater. Sci.*, **27** (1992) 4429.
12. BOUTZ, M. M. R., WINNUBST, A. J. A. & BURGGRAAF, A. J., *J. Eur. Ceram. Soc.*, **13** (1994) 103.
13. ASHBY, M. F. & VARREL, R. A., *Acta Metall.*, **21** (1973) 149.
14. YOSHIZAWA, Y. & SAKUMA, T., *J. Am. Ceram. Soc.*, **73** (1990) 3069.
15. VAN DIJK, T. & BURGGRAAF, A. J., *Phys. Stat. Sol. A*, **63** (1981) 229.
16. BADWAL, S. P. S., CIACCHI, F. T., SWAIN, M. V. & ZELIZKO, V., *J. Am. Ceram. Soc.*, **73** (1990) 2505.
17. VANGRUNDERBEEK, J., LUYTEN, J., KUYPERS, S., HENDRIX, W. & DE SCHUTTER, F., *Electrochim. Acta*, **38** (1993) 2099.
18. VERKERK, M. J., WINNUBST, A. J. A. & BURGGRAAF, A. J., *J. Mater. Sci.*, **17** (1982) 3113.
19. BOUTZ, M. M. R., WINNUBST, A. J. A., BURGGRAAF, A. J., NAUER, M. & CARRY, C., *J. Am. Ceram. Soc.*, **78** (1995) 121.
20. HE, Y. J., WINNUBST, A. J. A., VERWEIJ, H. & BURGGRAAF, A. J., *J. Mater. Sci.*, **29** (1994) 6505.
21. HE, Y. J., WINNUBST, A. J. A., VERWEIJ, H. & BURGGRAAF, A. J., *J. Mater. Sci.*, **29** (1994) 5868.
22. KRELL, A. & BLANK, P., *J. Eur. Ceram. Soc.*, **9** (1992) 127.
23. HE, Y. J., In Tribological and mechanical properties of fine-grained zirconia and zirconia–alumina ceramics. PhD thesis, University of Twente, The Netherlands, 1995.
24. HE, Y. J., WINNUBST, A. J. A., BURGGRAAF, A. J., VERWEIJ, H., VAN DER VARST, P. G. T. & DE WITH, G. submitted to *J. Eur. Ceram. Soc.*